Geodesy and Geodynamics 9 (2018) 246–251

Contents lists available at ScienceDirect

Geodesy and Geodynamics

journal homepage: http://www.keaipublishing.com/en/journals/geodesy-and-geodynamics/

Finite element modelling of the geodynamic processes of the Central Andes subduction zone: A Reference Model

Chris Salomon

Institute of Geosciences, General Geophysics and Structural Geology Group, Friedrich Schiller University, 07749, Jena, Burgweg 11, Germany

ARTICLE INFO

Article history:
Received 25 April 2017
Received in revised form
13 November 2017
Accepted 27 November 2017
Available online 3 February 2018

Keywords:
Abaqus
Andes subduction zone
Finite element modelling
Thermomechanical models
Viscoplasticity

ABSTRACT

This paper presents preliminary results of three-dimensional thermomechanical finite-element models of a parameter study to compute the current temperature and stress distribution in the subduction zone of the central Andes (16°S–26°S) up to a depth of 400 km, the bottom of the asthenosphere. For this purpose a simulation running over c. 50,000 years will be realized based on the geometry of a generic subduction zone and an elasto-viscoplastic Drucker–Prager rheology. The kinematic and thermal boundary conditions as well as the rheological parameters represent the current state of the study area. In future works the model will be refined using a systematic study of physical parameters in order to estimate the influence of the main parameters (e.g. viscosity, fault friction, velocity, shear heating) on the results of the reference model presented here. The reference model is kept as simple as possible to be able to estimate the influence of the parameters in future studies in the best possible way, whilst minimizing computational time.

1. Introduction

Subduction zone seismicity accounts for more than two thirds of the global seismic energy release (e.g. [1]) and is hence an integral process accompanying the recycling of lithospheric plates along convergent plate boundaries. Most subduction earthquakes, including 'giant' ones with moment magnitudes $Mw \geq 8$, are generated at intermediate depths between c. 50 and 300 km (e.g. [2]) and many factors have been invoked to explain their occurrence. The classical concept is that 'embrittlement' induced by metamorphic dehydration reactions in the downgoing slab is responsible for triggering intermediate depth seismic dislocations (e.g. [3,4]). 'Embrittlement' essentially means overcoming the brittle shear strength along the plate interface in the presence of a free fluid phase that counteracts normal stresses on faults. As an alternative mechanism for intermediate depth earthquakes, John et al. [5] and Prieto et al. [6] suggested that, in the absence of free fluids, so-called 'thermal runaway melting', induced by self-localising shear heating, might control seismogenic material failure at differential stresses lower than those needed for inducing brittle failure along a plate interface. Recent ideas on the occurrence of $Mw \geq 8$ earthquakes also suggested that they occur preferably along accretionary, i.e. addition of material to the overriding plate, rather than erosive margins, i.e. removal of material from the upper plate basement ([7] and references therein), implying that the presence vs. absence of large volumes of low-friction pelitic material constituting a trench-fill effectively controls fault friction and, in turn, when dynamically weakened during seismic slip ('velocity weakening' [8,9]), the size of the ruptured area and hence the seismic moment released along a subduction plate interface. However, the Tohoku $Mw = 9.1$ earthquake of 2011 [10] occurred along a clearly erosive subduction segment, rendering the notion of [7] at best contradictory and suggesting that possibly still other factors exert a control on where seismicity localises. The above examples highlight how strongly interdependent the rheological, geometrical and physical parameters (such as pressure, temperature as well as the presence vs. absence of volatile phases) are in triggering subduction zone seismicity; and controversies still prevail.

E-mail address: chris.salomon@uni-jena.de.

Peer review under responsibility of Institute of Seismology, China Earthquake Administration.

Production and Hosting by Elsevier on behalf of KeAi

https://doi.org/10.1016/j.geog.2017.11.007

This study addresses the temperature-dependent rheology of subducting lithosphere by means of three-dimensional numerical finite-element modelling using an elasto–viscoplastic rheological model, to obtain a better understanding of the stress distribution in subduction zones. For this the subduction zone of the central Andes (16°S–26°S) serves for scaling and calibration of the models (Fig. 1).

2. The reference model

The FEM (finite-element method) is a widely used technique among geophysicists for simulating plate movements along subduction zones. Using three-dimensional geometries enables us to do most realistic numerical simulations. However, these computations require very robust and time efficient numerical algorithms. This work therefore makes use of the FEM package Abaqus 6.14–2 [12], which is a widely accepted tool for a large range of applications in geosciences (e.g. www.ruhr-uni-bochum.de/geoqus). For testing purposes the geometry of the current reference model describes a generic subduction zone using a two-dimensional cross section extended to the third dimension (Fig. 2).

The size of the reference model is 650 km from west to east (x-direction), 400 km from south to north (z-direction) and 400 km from bottom to top (y-direction), resulting in approx. 27,000 three-dimensional finite elements. The boundary conditions (Fig. 3) applied include a constant gravitational acceleration acting on the overall model, the horizontal motion of the oceanic and continental plate, slab pull on the subducting slab into the lower earth's mantle, as well as friction including shear heating between the oceanic and continental crust along the plate interface (Fig. 3). During the simulation the eastern and western boundary elements of the asthenosphere are only allowed to move in vertical direction (y) while fixing the horizontal directions (x and z) to account for surrounding materials. The bottom of the oceanic as well as continental asthenosphere is completely fixed. The applied plate velocities are typical mean values according to Refs. [13–15]. The coefficient of friction along the plate interface was set to $\mu = 0.3$ down to the base of the upper plate Moho and $\mu = 0$ between the Moho and the lithosphere-asthenosphere boundary (LAB). This strict simplification was necessary for obtaining a numerically stable solution. In developing the models further, the author intends to modify the downdip variation in a more realistic way. The simulations intend to reflect the current subduction state before the occurrence of large earthquakes. To achieve this a dynamically stable equilibrium must be realized, which is considered to appear after c. 100,000 years of simulation duration. Due to this long-term effects such as erosion, convection and serpentinization in the forearc mantle are to be neglected.

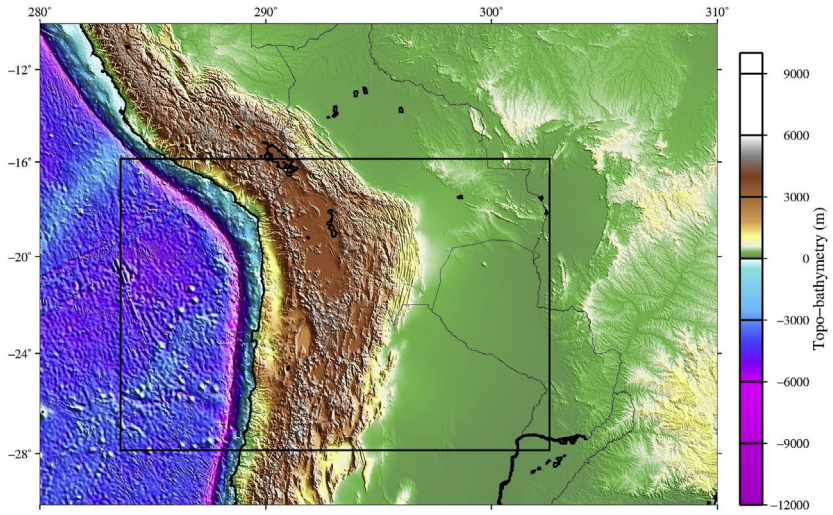

Fig. 1. Topographic map of the central Andes (conceived with Submap 4.0 [11]). The rectangle denotes the study area.

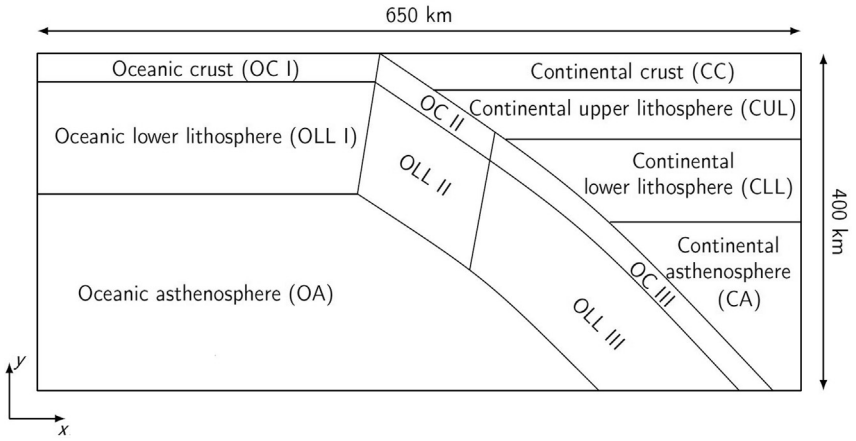

Fig. 2. Different parts of the model and their abbreviations.

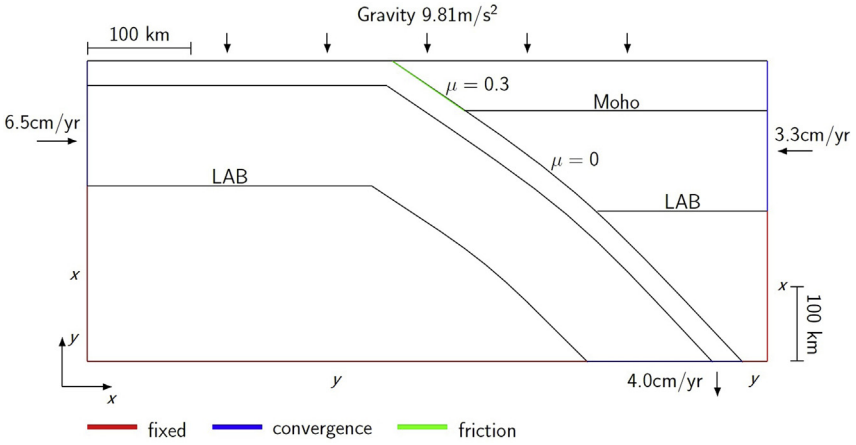

Fig. 3. 2D cross section through the reference model illustrating boundary conditions applied. LAB marks the lithosphere-asthenosphere boundary, Moho marks the Mohorovičić discontinuity.

To successfully integrate gravity a lithostatic stress distribution at the beginning of the simulation is needed. This is computed by additionally fixing the eastern and western boundary elements of the lithosphere in horizontal direction (x, z) and the bottom slab elements in vertical direction (y) for that gravity alone, as a load acting on all elements, determines the plate movements. On assuming an overall elastic rheology a static stress simulation is done by using the implicit FE method Abaqus/Standard (Fig. 4a). Furthermore a static temperature model is needed to complete the starting conditions. For simplicity this is currently achieved by defining isothermals for the top surface temperature (275 K), the continental Moho and lower boundary of the oceanic lithosphere (1523 K) as well as the bottom temperature (1873 K) of the model. In most studies a temperature of 1523 K is used at the LAB instead of at the continental Moho. But for the present model a constant temperature gradient of 30 °C/km was assumed resulting in the Moho temperature presented in this work. In upcoming models this value will be decreased to study its effect on the model results. Again Abaqus/Standard is used to compute the resulting temperature distribution (Fig. 4b).

The material parameters needed to define the rheology of the subduction model are taken from published theoretical and experimental studies and are presented in Table 1. For simplicity the Poisson ratio ν was set to a constant value of 0.25 although it is known to vary between c. 0.23 and 0.27 [16,17]. The thermal expansion coefficient α is also known to vary between c. $2-4\cdot10^{-5}K^{-1}$ [18,19] but for this reference model it was set to 0.0 K^{-1} in the overall model, to later be able to investigate its influences on the model results. The definitions of all parameters except the Poisson ratio ν, Young's modulus E and density ρ are given in section 3.

3. Drucker–Prager viscoplasticity

For describing thermo-mechanical processes one has to solve the coupled system of conservation equations for momentum (1), mass (2) and energy (3).

$$\frac{dv_i}{dt} = \frac{\partial \sigma_{ik}}{\partial x_k} + g_i \tag{1}$$

$$\frac{\partial \rho}{\partial t} + \frac{\partial}{\partial x_i}(\rho v_i) = 0 \tag{2}$$

$$\rho C_p \frac{dT}{dt} = \frac{\partial}{\partial x_i}\left(\kappa \frac{\partial T}{\partial x_i}\right) + \sigma_{ik}\frac{\partial v_k}{\partial x_i} + h \tag{3}$$

In these equations Einstein's summation rule applies and x_i are the coordinates, t –time, v_i –velocities, σ_{ik} –stress tensor, g_i –gravity vector, $d/dt = \partial/\partial t + (\partial/\partial x_j)\cdot(dx_j/dt)$ –material time derivative, ρ –mass density, C_p –heat capacity, κ –heat conductivity, h –internal heat generation.

By additionally solving the constitutive equations, which relate the stress to the strain tensor, all quantities are defined. This work uses a temperature dependent elasto-viscoplastic Drucker–Prager

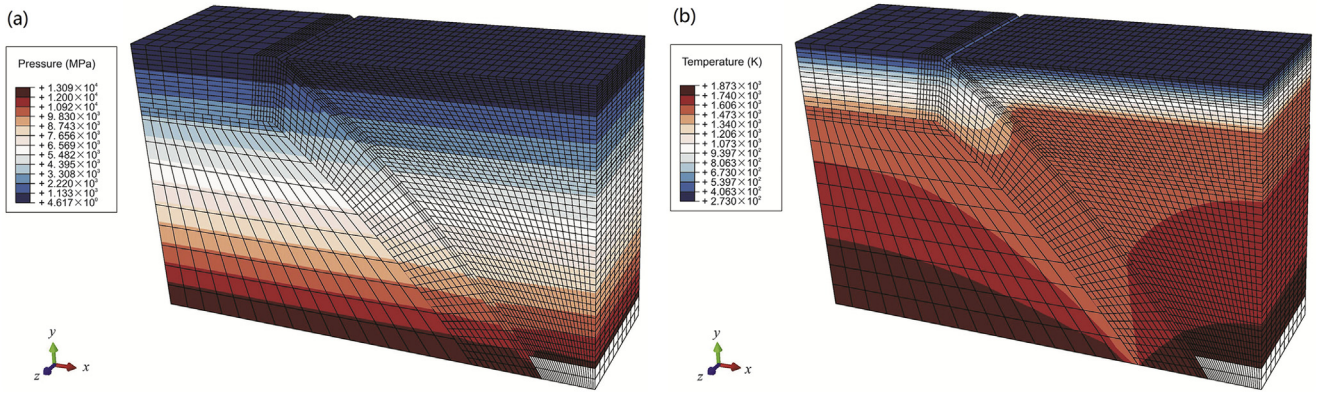

Fig. 4. Starting conditions of the model: a) Lithostatic pressure distribution in units of 1 MPa b) Static temperature distribution in units of 1 K.

Table 1
Rheological parameters used for the reference model: ν –Poisson ratio, ρ –mass density, E –Young's modulus, ϕ –internal friction angle, ϕ_{dil} –dilatancy angle, C –cohesion, N –power law coefficient, η_0 –viscosity at $T = T_{melt}$, E_A –creep activation energy, T_{melt} –melting temperature, α –linear thermal expansion coefficient, C_p –heat capacity, κ –heat conductivity; for abbreviations see Fig. 2.

Parameter	Model part	Value	Reference
ν	All	0.25	–
ρ (kg/m^3)	CC	2700	[20]
	CUL	3100	
	CLL	3320	
	CA	3430	
	OC I	3050	
	OLL I	3350	
	OC II	3300	
	OLL II	3400	
	OC III	3550	
	OLL III	3500	
	OA	3410	
E (GPa)	CC	80	[21]
	CUL	100	
	CLL	150	
	CA	180	
	OC I	98	
	OLL I	183	
	OC II	116	
	OLL II	186	
	OC III	125	
	OLL III	191	
	OA	205	
ϕ	ALL	40°	[22]
ϕ_{dil}	ALL	10°	[23]
C (MPa)	CC, CUL, OC I–III	20	[19,22,24]
	CLL, OLL I–III	30	
	CA, OA	50	
N	CC, CUL, CLL, OC I–III, OLL I–III	2.5	[22,25,26]
	CA, OA	3.5	
η_0 (MPa)	CC, CUL	$10^{}25$	[26]
	CLL	$10^{}22$	
	OC I–II	$10^{}27$	
	OLL I–III	$10^{}24$	
	CA, OA	$10^{}21$	
E_A (kJ mol^{-1})	CC, CUL, OC I–II	150	[22,26]
	OLL I–III, OC III	180	
	CLL, CA, OA	520	
T_{melt} (K)	CC, CUL, OC I–III, OLL I–III	2000	[27,28]
	CLL, CA, OA	2170	
α(K^{-1})	All	0.0	–
C_p(J kg^{-1} K^{-1})	CC, CUL, CLL, OC I-III, OLL I–III	1.7	[29,30]
	CA, OA	1.3	
κ(W m^{-1}K^{-1})	CC, CUL, CLL, OC I–III, OLL I–III	2.5	[22,30]
	CA, OA	6.9	

relationship in which the total strain rate is decomposed into elastic, viscoplastic and temperature components:

$$\dot{\varepsilon}_{ik} = \dot{\varepsilon}_{ik}^{(e)} + \dot{\varepsilon}_{ik}^{(v)} + \alpha\dot{T} \tag{4}$$

The viscoplastic components are defined by

$$\dot{\varepsilon}_{ik}^{(v)} = \dot{\lambda}\frac{\partial g}{\partial \sigma_{ik}} \tag{5}$$

with the Lagrangian multiplier $\dot{\lambda}$ and the plastic potential function $g = 2\sin\phi_{dil}/[\sqrt{3}(3-\sin\phi_{dil})]I_1 + \sqrt{J_2}$. $\dot{\lambda}$ is computed according to Alfano et al. [31] by solving the consistency condition

$$\mathrm{d}f = \mathrm{d}\Phi^{-1}\left(\dot{\lambda}\right) \tag{6}$$

with $f = 2\sin\phi/[\sqrt{3}(3-\sin\phi)]I_1 + \sqrt{J_2}$ –Drucker–Prager yield function, $\Phi^{-1}(\dot{\lambda})$ –inverse of Perzyna [32] overstress function $\Phi(f) = \sigma_{eff}(f/\sigma_Y)^N = \langle\eta\dot{\lambda}\rangle$, $<\ \ldots\ >$–McCauley brackets, ϕ_{dil} –dilatancy angle, ϕ –angle of internal friction, σ_{eff} –effective viscoplastic stress, $\sigma_Y = 6C\cos\phi/(3-\sin\phi)$ –yield stress, C –cohesion, N –power law coefficient, $\eta = \eta_0\exp[E_A/R(1/T - 1/T_{melt})]$ –viscosity, η_0 –viscosity at $T = T_{melt}$, E_A –creep activation energy, R –universal gas constant, T_{melt} –melting temperature, α –linear thermal expansion coefficient, I_1 –mean normal stress, J_2 –second invariant of deviatoric stress tensor.

On assuming isotropic linear elasticity the increments of the stress components are therefore given by

$$\mathrm{d}\sigma_{ij} = C_{ijkl}\left(\mathrm{d}\varepsilon_{kl} - \mathrm{d}\varepsilon_{kl}^{(v)}\right) \tag{7}$$

with the elastic stiffness tensor

$$C_{ijkl} = \mu\left(\delta_{ik}\delta_{jl} + \delta_{il}\delta_{jk}\right) + \lambda_L\delta_{ij}\delta_{kl} \tag{8}$$

where μ –shear modulus or second Lamé constant, λ_L –first Lamé constant, δ_{ik} –identity tensor. Given the Poisson ratio ν and Young's modulus E the Lamé constants are defined by

$$\mu = \frac{E}{2(1+\nu)} \tag{9}$$

$$\lambda_L = \frac{E\nu}{(1+\nu)(1-2\nu)} \tag{10}$$

4. Results and discussion

The final simulation of the current subduction reference model is carried out using the explicit FE method Abaqus/Explicit. Due to this several 100,000's of time increments are needed to achieve a dynamic equilibrium state of the subduction process. Numerical uncertainties, e.g. because of round off errors, can thus have a significant influence on the stability of the computation. Currently the models are able to simulate up to c. 50,000 years of subduction using the conditions described in section 2, which is considered to be the minimum simulation duration to achieve the acquired equilibrium.

Fig. 5 shows the final distributions of the translation in y-direction (i.e. upwards), the pressure, the heat flux as well as the temperature in the model. The model has an increasing downwards translation towards the trench (Fig. 5a). Especially the subducting oceanic plate is downlifted by several kilometres. According to observations of subduction zones in reality one would expect uplifting of near trench regions of the continental instead of downlifting of the oceanic plate. The reasons for this discrepancy maybe the steep dipping angle of the slab of up to 50° at the bottom of the model, the low depth of the continental Moho of 40 km or the missing horizontal component of the slab pull velocity.

The pressure gradient of the continental plate has decreased during the subduction process in comparison to the gradient of the oceanic plate (Fig. 5b). In the bottom of the model, between slab and continental asthenosphere, a high pressure has been accumulated. The left and right ends of the model are dominated by boundary effects. In the uppermost layer of the continental crust tensional stresses are present around the trench. This is considered to be another boundary effect because no corresponding uplifting can be seen in Fig. 5a. The oceanic asthenosphere is dominated by artefacts due to the coarse mesh. Nevertheless the overall pressure is lower than in the continental asthenosphere.

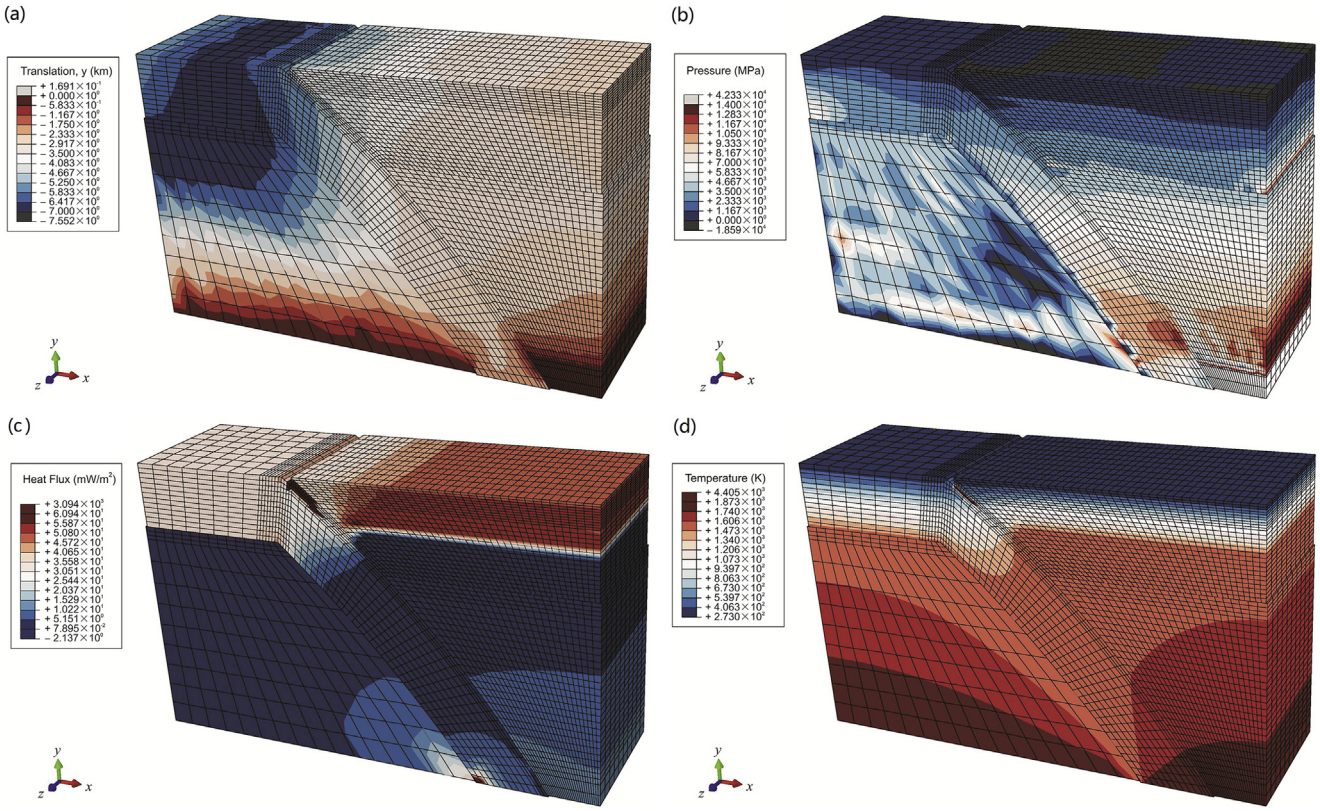

Fig. 5. Final results of the simulation after c. 50,000 years of subduction. a) Translation in y- (i.e. upwards-) direction in units of 1 km; b) pressure in units of 1 MPa; c) heat flux magnitude in units of 1 mW/m^2; d) temperature in units of 1 K.

The heat flux magnitude (Fig. 5c) in the oceanic lithosphere is nearly constant while in the continental lithosphere the heat flux down to the Moho is significantly higher than in the lower lithosphere. Below the depth of the Moho the heat flux decreases significantly in the lower continental lithosphere and overall asthenosphere but with increasing depth a slight increase can be observed. Furthermore around the frictional coupling zone of the plates a very high heat flux is observed being two magnitudes higher than in the surroundings, resulting in an increase of the temperature to more than 4000 K (Fig. 5d) which is clearly the effect of shear heating in the model. These values are quite high and have to be improved in future model runs by adjusting different parameters such as the friction coefficient and the dipping angle of the slab. All remaining parts of the temperature distribution have hardly changed in comparison to the starting distribution (Fig. 4b).

5. Conclusions

In this work a three-dimensional thermomechanical finite element model of a generic subduction zone was created using available data from the subducting region around the central Andes. The current reference model already includes all boundary conditions as well as material properties belonging to the desired region and shows a dynamically stable subduction process of up to c. 50,000 years. Despite the geologically short simulation duration the model already starts being in a dynamically stable equilibrium including shear heating in the frictional coupling zone, a change in the pressure gradient between the continental and oceanic plate and vertical movements of the plates. Thus the model presented here can already serve as reference model for a subsequent parameter study. During this parameters such as the dipping angle of the slab, the friction coefficient, downdip limit, viscosity and the amount of shear heating will be refined to estimate their influence on the results of the reference model.

Acknowledgements

I greatly appreciate Thomas Jahr, Kamil Ustaszewski and the structural geology team for very constructive discussions and helpful hints related to this work.

References

[1] J.F. Pacheco, L.R. Sykes, Seismic moment catalog of large shallow earthquakes, 1900 to 1989, Bull. Seism. Soc. Am. 82 (3) (1992) 1306–1349.
[2] S. Stein, M. Wysession, An Introduction to Seismology, Earthquakes and Earth Structure, Blackwell Publishing, 2005.
[3] H.W. Green, H. Houston, The mechanics of deep earthquakes, Ann. Rev. EPS 23 (1) (1995) 169–213.
[4] B.R. Hacker, S.M. Peacock, G.A. Abers, S.D. Holloway, Subduction factory 2. Are intermediate-depth earthquakes in subducting slabs linked to metamorphic dehydration reactions?, J. Geophys. Res. 108 (B1) (2003), https://doi.org/10.1029/2001JB001129.
[5] T.S. John, S. Medvedev, L.H. Rupke, T.B. Andersen, Y.Y. Podladchikov, H. Austrheim, Generation of intermediate-depth earthquakes by self-localizing thermal runaway, Nat. Geosci. 2 (2) (2009) 137–140, https://doi.org/10.1038/ngeo419.
[6] G.A. Prieto, M. Florez, S.A. Barrett, G.C. Beroza, P. Pedraza, J.F. Blanco, E. Poveda, Seismic evidence for thermal runaway during intermediate-depth earthquake rupture, Geophys. Res. L. 40 (23) (2013) 6064–6068, https://doi.org/10.1002/2013GL058109.
[7] S.L. Bilek, The role of subduction erosion on seismicity, Geology 38 (2010) 479–480, https://doi.org/10.1130/focus052010.1.
[8] C. Marone, C.H. Scholz, The depth of seismic faulting and the upper transition from stable to unstable slip regimes, Geophys. Res. L. 15 (6) (1988) 621–624, https://doi.org/10.1029/GL015i006p00621.

[9] K. Ujie, G. Kimura, Earthquake faulting in subduction zones: insights from fault rocks in accretionary prisms, Prog. EPS 1 (1) (2014) 7, https://doi.org/10.1186/2197-4284-1-7.
[10] D. Bassett, D.T. Sandwell, Y. Fialko, A.B. Watts, Upper-plate controls on co-seismic slip in the 2011 magnitude 9.0 Tohoku-Oki earthquake, Nature 531 (2016) 92–96, https://doi.org/10.1038/nature16945.
[11] A. Heuret, S. Lallemand, Plate motions, slab dynamics and back-arc deformation, PEPI 149 (2005) 31–51, https://doi.org/10.1016/j.pepi.2004.08.022.
[12] Dassault Systèmes SIMULIA, 2017. http://www.3ds.com. (Accessed 20 April 2017).
[13] E. Norabuena, L. Leffler-Griffin, A. Mao, T. Dixon, S. Stein, I.S. Sacks, L. Ocola, M. Ellis, Space geodetic observations of nazca-south America convergence across the central Andes, Science 279 (1998) 358–362, https://doi.org/10.1126/science.279.5349.358.
[14] E. Kendrick, M. Bevis, R. Smalley Jr., B. Brooks, R.B. Vargas, E. Lauría, L.P.S. Fortes, The Nazca-South America Euler vector and its rate of change, J. S. Am. Earth Sci. 16 (2003) 125–131, https://doi.org/10.1016/S0895-9811(03)00028-2.
[15] E.M. Syracuse, P.E. van Keken, G.A. Abers, The global range of subduction zone thermal models, PEPI 183 (2010) 73–90, https://doi.org/10.1016/j.pepi.2010.02.004.
[16] I. Koulakov, S.V. Sobolev, G. Asch, P- and S-velocity images of the lithosphere-asthenosphere system in the Central Andes from local-source tomographic inversion, Geophys. J. Int. 167 (2006) 106–126, https://doi.org/10.1111/j.1365-246X.2006.02949.x.
[17] Y. Dzierma, W. Rabbel, M. Thorwart, I. Koulakov, H. Wehrmann, K. Hoernle, D. Comte, Seismic velocity structure of the slab and continental plate in the region of the 1960 Valdivia (Chile) slip maximum – insights into fluid release and plate coupling, EPSL 331–332 (2012) 164–176, https://doi.org/10.1016/j.epsl.2012.02.006.
[18] J.C. Afonso, G. Ranalli, M. Fernandez, Thermal expansivity and elastic properties of the lithospheric mantle: results from mineral physics of composites, PEPI 149 (2005) 279–306, https://doi.org/10.1016/j.pepi.2004.10.003.
[19] A.Y. Babeyko, S.V. Sobolev, High-resolution numerical modelling of stress distribution in visco-elasto-plastic subducting slabs, Lithos 103 (2008) 205–216, https://doi.org/10.1016/j.lithos.2007.09.015.
[20] A. Tassara, H.-J. Götze, R. Hackney, Three-dimensional density model of the Nazca plate and the Andean continental margin, J. Geophys. Res. 111 (B9, 404) (2006), https://doi.org/10.1029/2005JB003976.
[21] ANCORP Working Group, Seismic imaging of a convergent continental margin and plateau in the central Andes (Andean Continental Research Project 1996/ANCORP'96), J. Geophys. Res. 108 (B7) (2003) 2328, https://doi.org/10.1029/2002JB001771.
[22] G. Ranalli, Rheology of the Earth, Chapman and Hall, 1995. ISBN: 0-412-54670-1.
[23] P.N. Michelis, Work-softening and hardening behaviour of granular rocks, Rock Mech. 14 (1981) 187–200, https://doi.org/10.1007/BF01250450.
[24] S. Zeumann, 3D Finite Element Modelling of the Central Andean Subduction Zone with Realistic Geometry (Ph.D. Thesis), Friedrich-Schiller University, Jena, Germany, 2013.
[25] P. Wu, Deformation of an incompressible viscoelastic flat earth with power-law creep: a finite element approach, Geophys. J. Int. 108 (1992) 35–51, https://doi.org/10.1111/j.1365-246X.1992.tb00837.x.
[26] S.-I. Karato, Rheology of the deep upper mantle and its implications for the preservation of the continental roots: a review, Tectonophysics 482 (2010) 82–98, https://doi.org/10.1016/j.tecto.2009.04.011.
[27] L.M. Barron, Thermodynamic multicomponent silicate equilibrium phase calculations, Am. Mineral. 57 (1972) 809–823.
[28] D.C. Presnall, M.J. Walter, Melting of forsterite, Mg2SiO4, from 9.7 to 16.5 GPa, J. Geophys. Res. 98 (B11) (1993) 19777–19783, https://doi.org/10.1029/93JB01007.
[29] R.G. Berman, L.Y. Aranovich, Optimized standard state and solution properties of minerals: 1. Model calibration for olivine, orthopyroxene, cordierite, garnet and ilmenite in the system FeO-MgO-CaO-Al2O3-TiO2-SiO2, Contrib. Mineral. Petrol. 126 (1996) 1–24, https://doi.org/10.1007/S004100050232.
[30] A.G. Whittington, A.M. Hofmeister, P.I. Nabelek, Temperature-dependent thermal diffusivity of the Earth's crust and implications for magmatism, Nature 458 (2009) 319–321, https://doi.org/10.1038/nature07818.
[31] G. Alfano, F. De Angelis, L. Rosati, General solution procedures in elasto/viscoplasticity, Comput. Meth. Appl. Mech. Eng. 190 (2001) 5123–5147, https://doi.org/10.1016/S0045-7825(00)00370-4.
[32] P. Perzyna, Fundamental problems in viscoplasticity, Red. Adv. Appl. Mech. 9 (1966) 243–377.

Chris Salomon, 2007 to 2013 Friedrich-Schiller-University Jena (FSU), Physics Diploma
2013–2014 research assistant at Institute of Gesciences FSU (IGW)
Since 2014 PhD candidate at IGW.